Response Characteristics of Flush End-Plate Connections

Ahmed Elkady

Lecturer in Structural Engineering, Department of Civil, Maritime and Environmental Engineering, University of Southampton, United Kingdom (e-mail: a.elkady@soton.ac.uk)

Abstract

Flush end-plate (FEP) connections are one of the most popular bolted steel connections in construction practice. These connections possess a semi-rigid moment-rotation behavior that betwixt that of rigid and pinned connections. Nonetheless, they are commonly idealized as pinned connections in design and numerical simulations. This paper investigates the flexibility, strength and ductility of such connections in a holistic manner, based on a recently compiled comprehensive database of more than 420 specimens that were tested within the past 50 years. The paper describes the systematic methodology used to deduce response parameters from the moment-rotation curves. This includes the deduction of the elastic, post-yield stiffnesses, effective yield and maximum moments as well as the ultimate rotations at failure. The deduced parameters are made publically available to support further analysis by other researchers. The median value of each parameter and associated variability is quantified with respect to different connection topologies and loading histories. The data are then used to assess the connection classification and performance in terms of flexibility, strength and ductility based on existing standards.

Keywords

Steel connections; Semi-rigid; Partial-strength; Flush end-plate; Moment-rotation; Eurocode 3

This article is cited as:

Elkady, A. (2022). "Response characteristics of flush end-plate connections." Engineering Structures, 269, DOI: 10.1016/j.engstruct.2022.114856.

1 Introduction

Semi-rigid (SR) beam-to-column and beam-to-beam connections are commonly used in steel framing worldwide. These connections are expected to develop moderate rotational stiffness and flexural capacity, that fall between the two ideal cases of pinned (or simple) and rigid (or fully-rigid) connections as illustrated in Figure 1a. Unlike fully-rigid connections, where plastic deformations predominantly occur in the beam, plastic deformations in semi-rigid connections take place in the connected components (i.e., column flange, angle cleat, end-plate, shear-tab and bolts). Among the different types of SR connections, flush end-plate (FEP) connections –the focus of this study- are the most abundant in construction practice. FEP connections can develop a relatively large stiffness and flexural capacities, compared to other SR connection types. These connections generally develop a nonlinear power-shaped moment-rotation response up to failure. This nonlinear response is governed by the elastic and plastic deformations of the connections elements including the bending of the end-plate, the elongation of bolts, the bending of the column flange, the shear deformation of the column web (i.e., panel zone) and, in limited cases, the concurrent buckling of the beam flange/web as demonstrated in Figure 1b.

FEP connections are extensively studied in literature both experimentally and numerically. These studies generally focused on investigating the effect of one or more geometric, material or loading parameters on the connection response. The findings of these studies provided valuable insights into the performance of different FEP connection topologies. While these studies were focused in their scope, to the best of the author's knowledge, no studies aimed at assessing the connection performance in a holistic manner, considering the wide range of possible connection topologies and designs. Understanding the characteristics of the connection behavior can assist the development of numerical modeling guidelines, performance acceptance criteria and damage fragilities, as part of the performance-based design framework. To that end, the objective of this study is to quantify the connection's characteristic response parameters and asses its response accordingly. This is accomplished by utilizing a recently complied comprehensive digital experimental database that comprises of more than 420 specimens [1]. This database constitutes a significant progress, in terms of number of collected specimens, tabulated test/specimen parameters and deduced response parameters, compared to previous attempts in the literature [2-6]. This allows for more inclusive and generalized observations.

In the following sections, the systematic methodology for fitting a trilinear curve to the moment-rotation test data and for deducing the different response parameters (including stiffness, strength and ductility parameters) is described. The fitted curves and parameters database are made available publicly online. The magnitude and variability in each response parameter are then quantified and discussed based on the connection topology and loading history. The data is also used to classify the connection with respect to rigidity and strength, based on both the European and American standards.

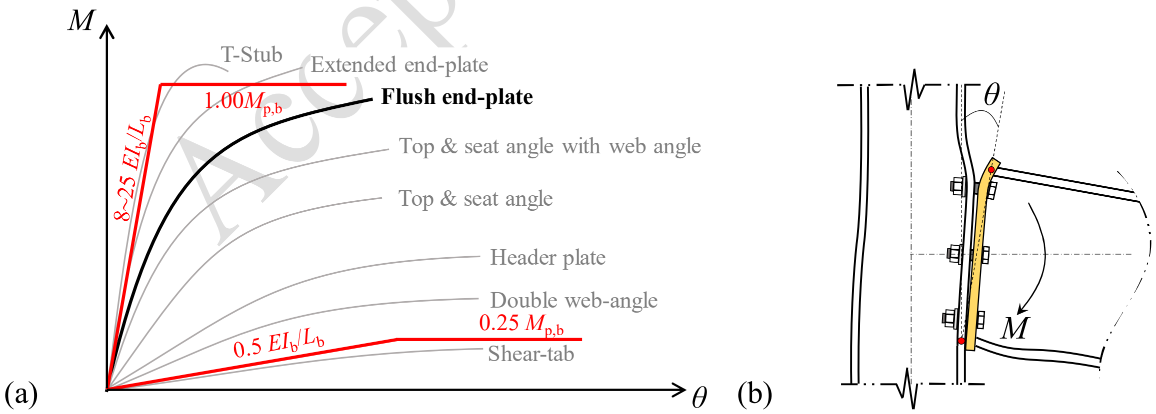

Figure 1. (a) Illustration of typical moment-rotation responses of SR connections and their expected classification based on Eurocode 3; (b) general deformed shape of an FEP connection

2 Experimental Database

A comprehensive experimental database on bare steel and composite FEP connection was recently complied and made publically available [1]. The current version of the database includes the geometric and material parameters of 427 specimens from 71 different testing programs as well as their moment-rotation responses in digital form. The specimens include both beam-to-column and beam-to-beam (splice) connections. Splice connections are considered herein as they are analogous to beam-to-column connection where the column is practically rigid. Table 1 provides a breakdown of the number of tests based on connection topology and loading history. In summary, the majority of these specimens are bare steel connections that were tested monotonically while only 80 specimens were tested cyclically and 77 are composite connections. The database uniformly covers a wide-range of FEP connections' design space that is commonly used in practice, with shallow (~100mm) to deep (~900mm) beams and thin (~6mm) to thick (~35mm) end-plates. Connections with 4, 6 and 8 bolt configurations are included. Several specimens were fabricated from high strength steel and stainless steel grades. For full details regarding the database, please refer to Mak and Elkady [1].

Table 1. Breakdown of database based on joint topology and loading type

Joint/Loading type	**Number of tests**
Bare steel with I-shaped columns	305
Bare steel with HSS columns	45
Bare steel splices	52
Composite with I-shaped columns	56
Composite with HSS columns	21
Minor-axis	18
Monotonic loading	347
Cyclic loading	80

3 Deduction of Response Parameters

Figure 2 shows an illustration of a typical moment-rotation (M-θ) curve of an FEP connection under monotonic loading. In the case of cyclic loading, this curve represents the average cyclic envelope of both the positive and negative loading directions. For consistency with past experimental and numerical research, moment is defined as the moment at the column face and the rotation is defined as the joint rotation resulting from the shear deformation of the column web, bending deformation of the column flange, plastic local deformation of the beam web/flange, elongation on the bolts and bending deformation of the end plate. In other words, the rotation represents the total rotation of the joint minus the rotation components resulting from the elastic shear/flexural deformations of the beam and the column.

It is worth noting that in steel frame analysis, the joint can be idealized in several ways in practice. This includes: 1) using a single spring at the column face with rigid offset elements from the column center, 2) using a single spring at the column center, and 3) a spring for the column panel zone at column center plus a spring for the connection at column face. Any of these approaches are valid as long as the spring(s) moment-rotation definitions are consistent with the assumptions made in the global analysis of the structure. The moment-rotation definition here in, can be used directly in lieu with the option 1. It can also be used with the other options with simple modifications to the stiffness and strength response quantities. For example, for option 2, the moment can be projected to the column center (about 3%~10% increase). For option 3, the panel zone flexibility need to be removed from the joint rotation.

Key moment-rotation response parameters are deduced from the test data. This is done by fitting the response curve with a trilinear curve as illustrated in Figure 2. The deduced parameters include the elastic and post-yield rotational stiffnesses (K_e and K_s, respectively), the yield, effective yield, maximum and capping moments (M_y, M_{ye}, M_{max}, and M_c respectively), and the plastic, post-capping and failure rotations (θ_p, θ_{pc} and θ_f, respectively). The method used to deduce each parameter is discussed next in detail.

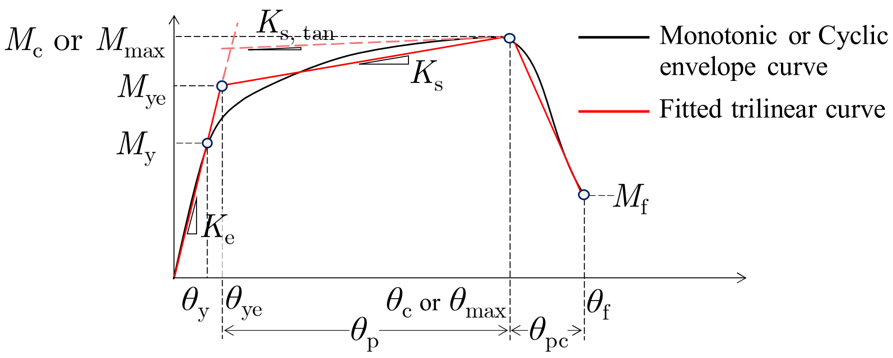

Figure 2. Trilinear fitting of the moment-rotation response and deduced parameters

The first parameter to be deduced is the elastic rotational stiffness K_e. The elastic stiffness can be sensitive to the employed deduction method. This is especially true when dealing with responses with highly nonlinear or ill-defined elastic regions which result from slippage, friction or setup vibrations. For that reason, three methods are used to estimate K_e as demonstrated in Figure 3. In the first method K_e is simply deduced by conducting linear regression on the data points preceding 30% M_{max}. The 30% M_{max} level was chosen based on a preliminary evaluation of the response data. Ideally, the data point at the onset of yielding would be used instead, however, this is not always reported by researchers and not easily inferred with confidence from the data. In the second method, the secant stiffness at each data point is evaluated and K_e is taken based on the point beyond which the secant stiffness changes by more than 20% compared to the average secant stiffness of the preceding points. Similarly, in the third method, the incremental (instead of the secant) stiffness is computed at several points and K_e is taken based on the point beyond which the incremental stiffness changes by more than 30% compared to the average incremental stiffness of the preceding points. Finally, the median value of the three methods' estimates is considered. Note that the response curve of each specimen was refined and divided into a consistent 100 data points prior to fitting to ensure the consistency of the aforementioned methods across different specimens. Also, the three methods typically result in similar values with variation less than 15%. In very limited cases, where the aforementioned methods failed (i.e., variation between the different methods is more than 15%) when the elastic region is not smooth or has sudden load reversals, K_e was deduced manually in a subjective manner.

Knowing K_e, the yield moment, M_y, is deduced as the point at which the nonlinear response deviates from the elastic slope. Quantitatively, this is taken as the point where the moment difference between the elastic slope and the response curve exceeds 10%, as illustrated in Figure 4a. Alternatively, M_y can be deduced based on the difference in rotation. Although both approaches are valid, the former is more convenient since the change in moment is more evident (refer to Figure 4a). Next, the connection moment capacity is deduced. Note here that several tests stopped prior to reaching the connection capacity, hence, a distinction is made here between the maximum and capping moments. The former (M_{max}) represents the maximum moment reached during the test while the latter (M_c) represent the true moment capacity of the connection after which strength deteriorates. Following, the post-yield stiffness (i.e., hardening slope), K_s, is deduced. As shown in Figure 4b, K_s is the post-yield stiffness at which the two areas enclosed by the hardening slope and the response data, between M_y and M_{max}, are equal (i.e., the equal-area fitting method). The effective yield moment, M_{ye}, is taken as the intersection point between the elastic slope and hardening slope. The term "effective yield moment" is commonly used in literature and is analogues to the plastic moment capacity of the connection [7-9]. It is important to note that in tests that did not reach their true ultimate capacity (capping point), M_{ye} as currently defined will be slightly conservative since the majority of tests reached rotations larger than 3%; after which the post-yield slope remains almost constant (refer to Figure 6a). Therefore, although there will be a difference, it is not significant (<15%).

Finally, the failure rotation is deduced. Note that many tests stopped prior to reaching true failure (visible loss of strength due to failure of one or more components). Also, failure in SR connections (mainly due to bolt or weld fracture) mostly occurs right after the attainment of the maximum moment; hence, the drop in strength is sudden. Limited number of tests reached a capping moment and experienced a recognizable post-capping negative slope prior to failure, as will be discussed later on in detail. Figure 5 shows couple of curve fitting examples of two specimens with and without a post-capping zone. All specimens' fitted curves and values of fitted parameters are publically accessible through the interactive SR connection database explorer, *SRConED*, which is available on GitHub [1].

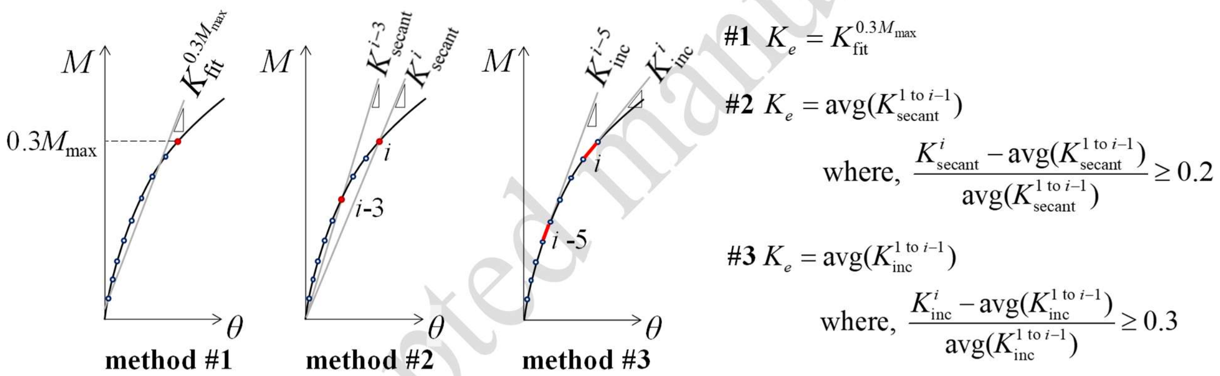

Figure 3. Methods used in deducing the elastic rotational stiffness

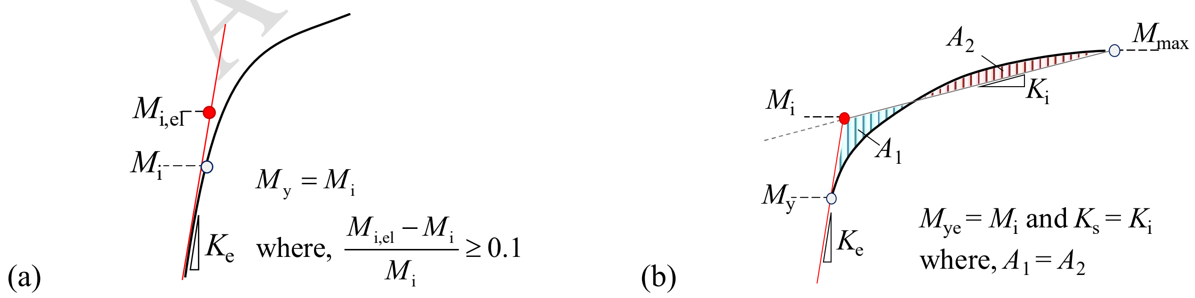

Figure 4. Methods used in deducing (a) M_y and (b) K_s and M_{ye}

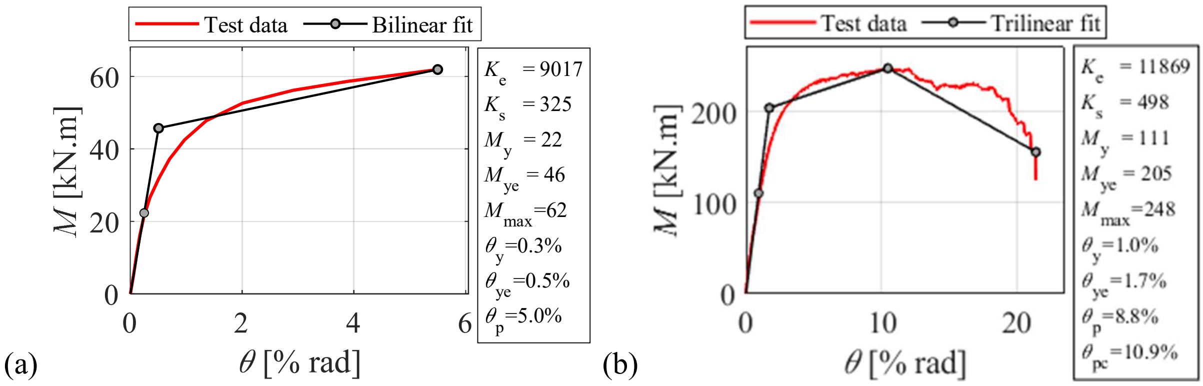

Figure 5. Examples of test data fitting: (a) Test 1 by Ostrander [10]; (b) Test 1-2A by Qiang et al. [11]

4 Connection Response Characteristics

In this section, the FEP connection basic characteristics are assessed based on the deduced response parameters including its stiffness, flexural strength and ductility.

4.1 Connection Classification

As per Eurocode 3 Part 1-8 [12] classification, a connection can be classified as semi-rigid if its strength falls between 0.25 and 1.0 $M_{p,b}$, and its stiffness between 0.25 and 8 EI_b/L_b (or 25 EI_b/L_b for joints in unbraced/non-sway frames), where $M_{p,b}$ is the beam plastic flexural strength, E_b is the measured elasticity modulus of the beam's material, I_b is the beam's second moment of inertia about the section's major axis, and L_b is the beam's length between column centerlines. AISC 360-16 [13] specifies similar limits. Particularly, stiffness shall fall between 2 and 20 EI_b/L_b, regardless of the frame sway condition. With respect to strength, only a lower bound is specified that is at least 0.2 $M_{p,b}$ at a joint rotation of 2%.

Figure 6 shows a plot of all the collected M-θ responses superimposed by the classification boundaries of Eurocode 3 and AISC 360-16. To allow for such plot, the moment is normalized by $M_{p,b}$ (based on the measured material properties) and the rotation is normalized by the reference plastic rotation θ_{pr} which is computed as $M_{ye}/(EI_b/L_b)$, where L_b is assumed as 15 h_b. This assumption is reasonable at it results in realistic beam lengths with respect to the beam depth h_b. Also note that these responses are only plotted up to the maximum moment, with the post-capping range trimmed, to improve visuals. Based on this figure, FEP connections cover a wide range of responses, falling within all three classification categories. The majority of tests fall within the semi-rigid range. Notably, and as expected, bare steel FEP connection with minor-axis orientation (i.e., beam connected to column web) possess the lowest stiffness and strength owing to the high deformability of the column web in transverse bending. On the other hand, composite FEP connections achieves the largest stiffness and strength which can sometimes places them within the fully-rigid/full-strength category. Note here that the composite response referred to herein is the one under hogging moment (i.e., slab is in tension). The specific parameters of these responses are quantified and assessed in detail in the following sections.

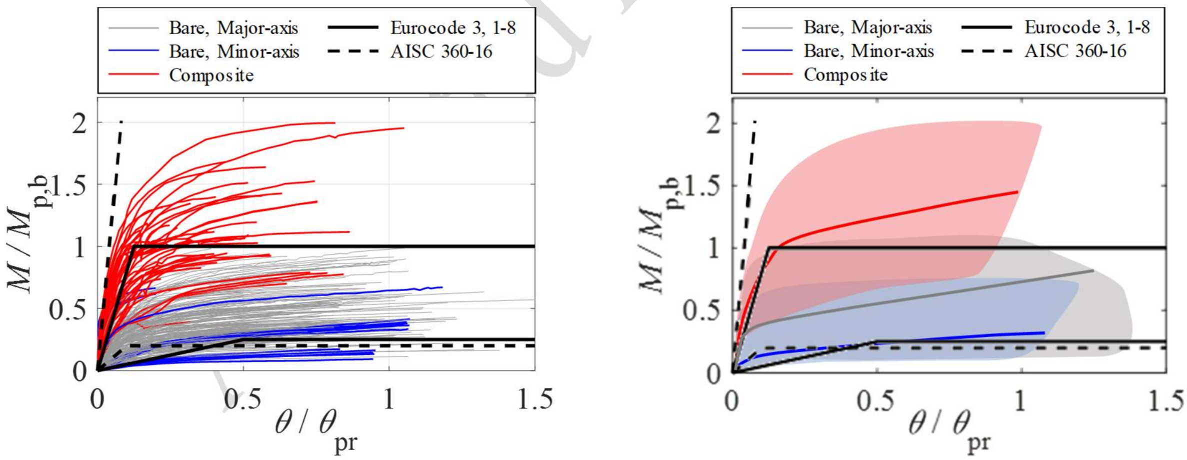

Figure 6. Normalized moment-rotation responses of collected specimens: (a) individual test responses and (b) median and range of responses

4.2 Elastic rotational stiffness

Figure 7 shows the histogram of the rotational stiffness coefficient, $\beta = K_e/(EI_b/L_b)$ (y-axis represents the normalized count of occurrences). Note that the beam length changes among the different testing programs. In addition, for practical reasons and laboratory constraints, most test configurations utilize short beam lengths that are not representative of actual beam spans. This length however, has no effect on the moment-rotation behaviour, given that the elastic rotation of the beam is removed from the rotation definition as discussed earlier. Accordingly, and to maintain consistency, a reference beam length of 15 h_b is used to compute the β values, as discussed earlier.

This figure confirms the semi-rigid nature of bare steel FEP connections, with a median β value of 4.6 which falls almost mid-range between the pinned and fully-rigid connection limits based on Eurocode 3, Part 1-8 [12] (refer to Figure 1a). The stiffness increases when a composite slab is present. Composite connections develop a median β of 14.6 under hogging moment (e.g., Brown and Anderson [14]). This is due to the higher rigidity of the composite section. Similarly, large stiffness is expected in beam-to-beam (splice) connections with thick end-plates and fully pre-tensioned bolts (e.g., Srouji [15]). As such, splice FEP connections with thick end-plates as well as composite ones can be categorized as fully-rigid connections. On the lower end, β less than 2.0 is observed in minor-axis connections as well as connections with thin plates and unstiffened column flanges. It is important to note here that minor-axis interior connections (i.e., cruciform joints) subjected to symmetric loading develop large β values, since those are comparable to splice connections. This places them within the semi-rigid classification [16]. Those cases can be observed from the outlier minor-axis M-θ curves shown in Figure 6 and the β >10 values in Figure 7. One should note however that symmetric loading may be valid under uniform gravity loading conditions is not under lateral loads such as wind or earthquakes.

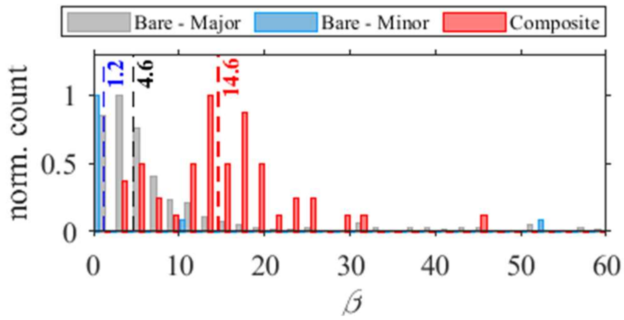

Figure 7. Distribution of the elastic stiffness coefficient

4.3 Effective yield (plastic) strength

The strength coefficient, α (where $\alpha = M_{ye}/M_{p,b}$), is used to quantify the connection's plastic strength. Figure 8a shows the histogram distributions of α based on the connection type. Bare steel FEP connections with major-axis orientation develop an appreciable median plastic strength of 0.32 $M_{p,b}$. As such they can be categorized as semi-rigid (or partial-strength) connections as per CEN [12] and AISC [13]. The same connections are able to carry up to 0.8 $M_{p,b}$ [17, 18]. Minor-axis connections, on the other hand, develop a lower plastic strength of 0.22 $M_{p,b}$ which places them within the pinned connection classification, with the exception of interior minor-axis connections under symmetric loading that developed $\alpha > 0.4$. Composite connections achieved more than double the strength of bare steel ones (median $\alpha = 0.83$). This is expected due to the increased lever arm and the additional tensile resistance of the tensile rebar and the steel deck. Many composite connections reached and exceed the beam bare flexural strength. This amplification becomes more evident in tests involving shallow beams (h_b<400mm) [19, 20].

Beyond the plastic strength, FEP connections can develop an ultimate/maximum strength that is 1.4 times larger than M_{ye}, on average, as shown in Figure 8b. Considering that some specimens did not reach their true ultimate strength as discussed earlier, this mean ratio is expected to be slightly higher (<10%). These observations underscore the potential economic savings that can be achieved in flexible (i.e., non-seismic) frame design, if the connection appreciable stiffness and strength are considered rather than the simplified pinned assumption. Similarly, in seismic regions where SR connections are used in gravity framing systems, it is important to consider their structural contribution in seismic evaluations. Past research showed that this contribution is significant and favorable to the building behavior [21, 22].

Finally, no difference is observed in the K_e and M_{ye} values with respect to the loading protocol (i.e., monotonic versus cyclic). The protocol however may affect the other response parameters in the plastic range, as discussed later on.

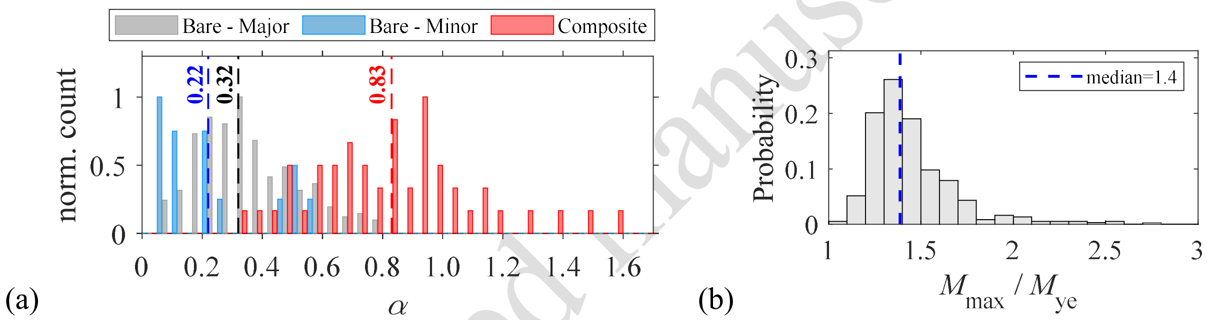

Figure 8. (a) Distribution of the strength coefficient (median values in dashed lines); (b) distribution of the maximum-to-effective-yield strength

4.4 Post yield (hardening) stiffness

SR connections are characterized with a smooth rounded transition from the elastic branch to the plastic branch. The plastic branch is almost linear slope, controlled by strain hardening. It is key to quantify the hardening slope, K_s, towards representative nonlinear model development rather than the conservative utilization of an elastic-perfectly-plastic one. Figure 9a shows that bare steel connections with major-axis orientation subjected to monotonic loading develop a median K_s/K_e value of 4%. This value corresponds approximately to a maximum-to-effective yield moment ratio (M_{max}/M_{ye}) of 1.35 (see Figure 8b). This relatively large hardening slope can be attributed to the fact that plastic deformations are contributed by non-deteriorating components such as the column web panel zone in shear and bolts in tension. This is consistent with values found in literature. For example, Davison et al. [23] observed that K_s is typically about 1/40 of K_e (i.e., K_s/K_e = 2.5%) by inspecting 54 bare steel major-axis connections. Also, 3% is commonly assumed for the hardening slope of the column web panel zone shear force-shear distortion [24, 25]. However, it worth noting that this M_{max}/M_{ye} ratio is slightly higher than the 1.1~1.2 value observed in welded steel beam-to-column, where beam buckling is the governing deformation mode [7, 20].

Minor-axis connections develop a large hardening slope of about 11%, primarily due to their low elastic stiffness values and high out-of-plane deformability of the column web. Connections undergoing cyclic loading also tend to develop larger K_s of about 8% K_e due to the combined effects of cyclic hardening and amplified strength. Lager K_s/K_e values (>15%) are observed in specimens with high strength steel (e.g., Coelho and Bijlaard [26]). Also, specimens fabricated from stainless steel grades tend to develop larger hardening slopes of about 7% K_e, (e.g., Elflah et al. [27]), compared to those fabricated from conventional steel grades.

It is worth noting the post-yield stiffness can be alternatively deduced based on the tangent slope ($K_{s,\ tangent}$) rather than the equal-area fit. As illustrated in Figure 10a. $K_{s,\ tangent}$ is deduced herein by linear fitting one-third of the discrete data points between M_{ye} and M_{max}, that are closest to M_{max}. The tangent slope is employed in literature by several researchers as well as in the European EQUALJOINTS project [28]. It is typically used in conjunction with the fitting of the Menegotto-Pinto and the modified four-parameter power model [29-31]. As shown in Figure 10b, $K_{s,\ tangent}$ values are roughly 30% lower than the K_s values discussed herein.

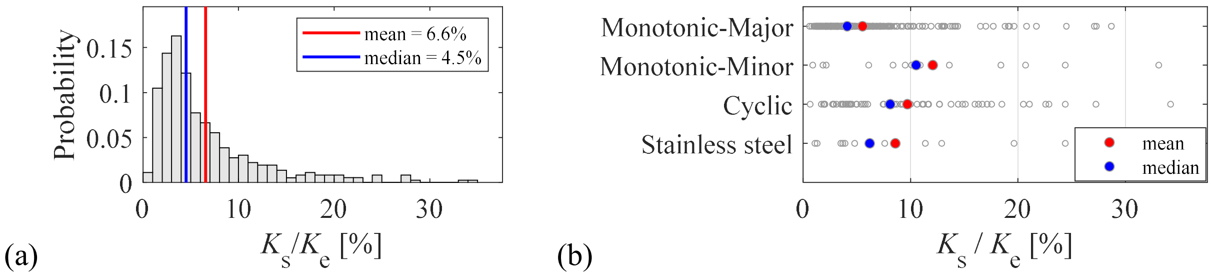

Figure 9. Distribution of the hardening-to-elastic slope ratio

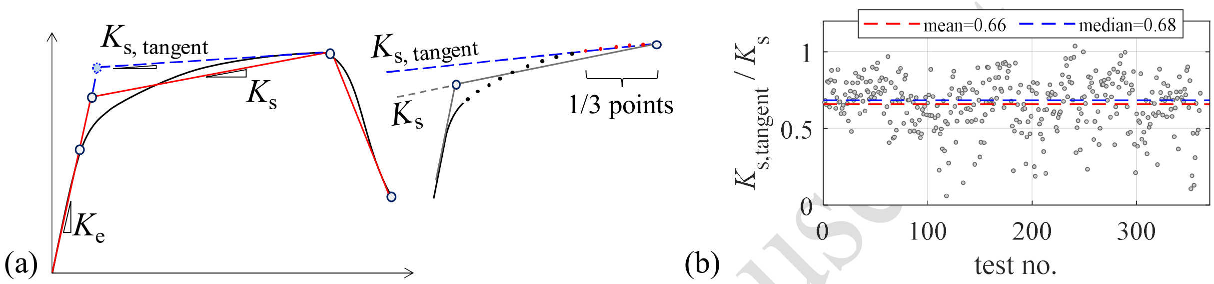

Figure 10. Post-yield stiffness deduced using the tangent and equal-area fitting methods

4.5 Yield moment and yield rotation

The onset of yielding, as defined earlier in Figure 4a, occurs mostly at rotations lower than 0.5% as shown in Figure 11a. In average, θ_y is 0.3%. This agrees with ASCE 41-17 [9] numerical modeling guidelines, which stipulates that SR connections possess an effective yield rotation, θ_{ye}, between 0.3% to 0.5%. When employing high strength steel with a high yield point, yield rotations can be as high as 1.5% (e.g., Qiang, Bijlaard et al. [11], Coelho and Bijlaard [26]). The yield moment is almost half the effective yield (plastic) moment as shown in Figure 11b. Specimens with yield strength close to the plastic one (i.e., M_y/M_{ye}>0.8) are typically those with a single deforming component, such as a thin end-plate or a thin column flange. In those cases, the component full plastification takes place right after yielding.

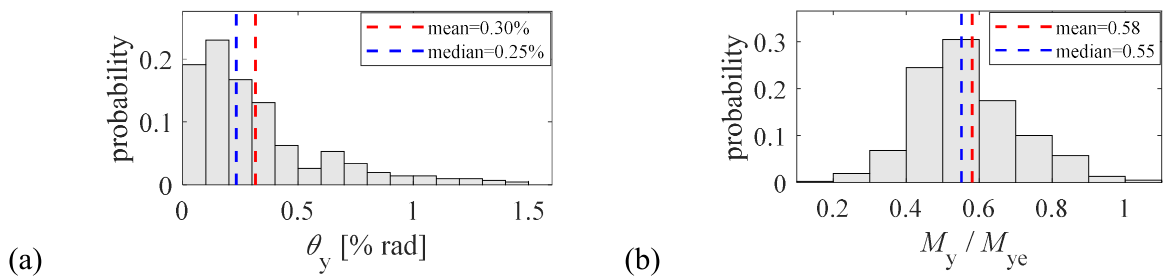

Figure 11. Distribution of the (a) yield rotation and (b) yield-to-effective yield strength ratio

4.6 Plastic rotation

Rotational ductility is a key response characteristic that needs to be available in critical structural members and joints for safe load transfer and load redistribution within a structure. The ductility of SR connections receives limited guidance in current standards. Herein, the plastic rotation capacity, θ_p, is used a direct measure of the connection's rotational ductility. Figure 12a shows that bare steel connections develop a median plastic rotation capacity of 4.1% which is comparable to fully-rigid connections [32]. This roughly corresponds to a median ductility level (θ_{max}/θ_{ye}) of 8. This level of ductility implies that FEP connections may be suitable for seismic applications, particularly for composite connections that can develop high stiffness and full beam moment capacity. Nonetheless, several bare steel connections still develop low plastic rotations of less than 1%. Those are mainly designed with stiffened columns and thick end-plates where the bolt elongation, stripping and/or rupture controls the deformation (i.e., mode 3 failure as per [12]). Note here that rotational ductility is generally inversely proportional to the elastic rotational stiffness. Minor-axis connections (specifically exterior joints) develop large median θ_p of 8.3% because their behavior is controlled by the out-of-plane bending of the column web, which is a ductile mode. Composite connections develop a lower median θ_p value of 2.4%. This is only due to the early drop in strength associated with concrete cracking and tensile rebar rupture.

It also observed from Figure 12a that the loading protocol does not affect the plastic rotation capacity. This is contrary to existing observations on fully-rigid welded beam-to-column connections [8, 33-35]. Fully-rigid connections' maximum strength is controlled by beam buckling which is triggered earlier under cyclic loading due to accumulated geometric imperfections. Semi-rigid connections, on the other hand, experience deformation modes that are not susceptible to imperfections. One should note however that reduced plastic rotation may result in some cases from degradation effects and fatigue failures associated with cyclic loading.

Improved ductility can be accomplished by the utilization of stainless steel grades. As shown in Figure 12b, stainless steel connection develop almost 60% larger plastic rotation compared to conventional steel.

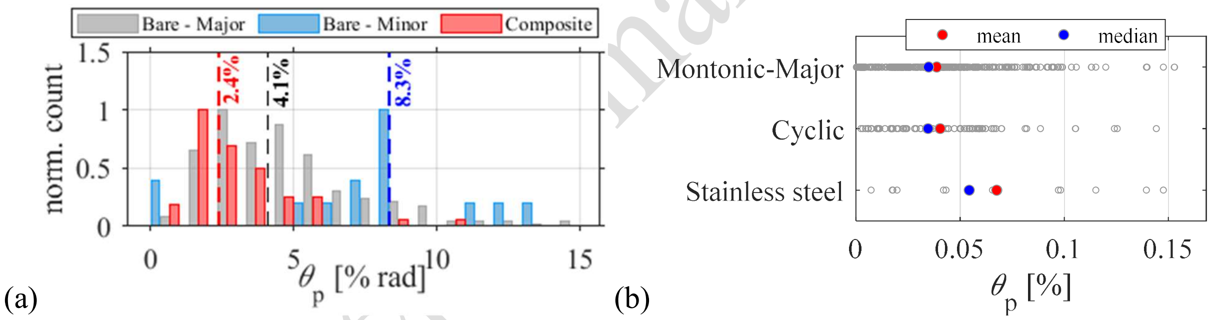

Figure 12. (a) Distribution of the plastic rotation; (b) scatter of the plastic rotation with respect to loading type

4.7 *Post-capping rotation*

Although FEP can develop an appreciable plastic rotational capacity as previously demonstrated, the level of rotational ductility post-the-capping point (after maximum strength is attained) is limited. This is because connection failure is generally coupled with the connection maximum strength (i.e., $\theta_f = \theta_{max} = \theta_c$). Moreover, most tests were stopped once excessive deformations took place, without reaching complete loss of strength. Out of all specimens, only 167 specimen reached failure (39%); hence, the post-capping rotation (θ_{pc}) could be quantified. These specimens are mostly composite connections or bare steel ones with bolt stripping as the failure mode. The histogram of θ_{pc} is shown in Figure 13. The median value is a modest 0.9%. For all practical reasons, it is reasonably conservative to assume that bare steel FEP connections do not possess any post-capping rotational capacity.

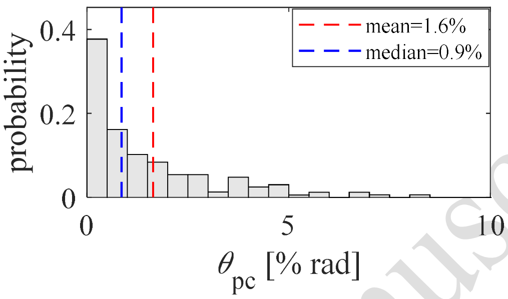

Figure 13. Histogram of the post-capping plastic rotation capacity

4.8 Failure rotation

As described earlier, failure in FEP connections takes place due to one of these modes: bolt rupture, bolt stripping, weld fracture or plate tearing. In composite connections, tensile rebar fracture and concrete crushing occur as well. Figure 14a shows the histogram of the failure rotation, θ_f, for the entire database. FEP connections mostly fail within a rotation range of 1% to 10% with a median failure rotation of 4.6%. This aggress with findings by Ostrowski and Kozłowski [36] who found it to range between 1.5% and 12%, based on parametric finite element simulation of stiffened FEP connections. Furthermore, the observed median θ_f agrees with ASCE 41-17 [9] guidelines, where an ultimate plastic rotation capacity of 4.2% is speculated for partially-restrained connections, assuming end-plate yielding controls the deformation. This becomes 1.2~1.8% when weld failure or bolt yielding is expected. This is also consistent with Eurocode 3 [12] which, although it does not provide quantitative values for the failure (ultimate) rotation, states that sufficient rotation capacity can be assumed as long as bolt or weld failure do not control the failure mode.

The majority of these failures (~70%) are due to bolt rupture, occurring at the attainment of the maximum moment. Early failures (θ_f < 2%) mainly took place in splice connections or in those with thick end-plates and/or stiffened columns. No difference is observed in θ_f with respect to loading protocol (monotonic versus cyclic), as shown in Figure 14b. This is due to the fact that fatigue-related failure modes (e.g., plate tearing) did not control the connection damage in most tests.

In summary, properly designed FEP connections (where, end-plate yielding is the controlling deformation mode and bolt and weld failures are avoided) are able to sustain reasonable rotations larger than 4.5% prior to failure. Furthermore, the utilization of stainless steel connections can improve the connection ductility and double failure rotation capacity to 10%. This, in combination with the improved plastic rotation capacity discussed earlier, demonstrates the potential applicability of such connection in progressive collapse prevention [37, 38] .

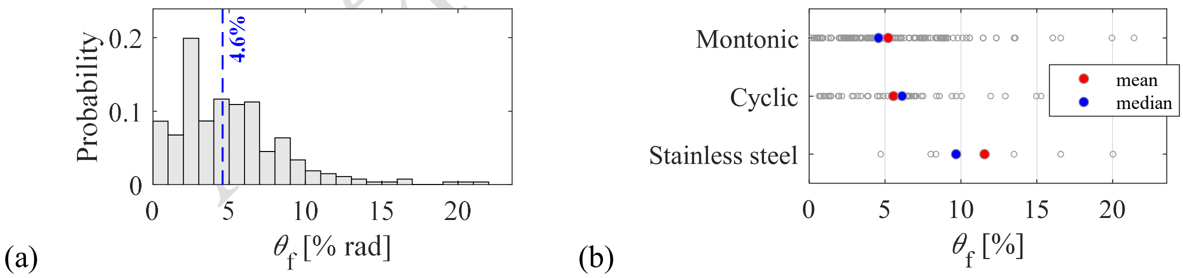

Figure 14. (a) Failure rotation histogram; (b) failure rotation scatter distribution based on load type and steel material

5 Summary and conclusions

The response characteristics of flush end-plate (FEP) connections are quantified and assessed based on a comprehensive experimental database comprising of 427 specimens. The following key observations are made:

- FEP connections can transmit 30% of the connected beam plastic moment capacity, on average, and up to 80%. These numbers are more than doubled in the presence of a composite concrete slab.
- As per the European [12] and American [13] standards' classification systems, bare steel FEP connections with major-axis orientation are semi-rigid/partially-restrained while exterior (single-sided) connections with weak-axis orientation are pinned. Composite connections featuring shallow beams can fall within the fully-rigid/fully-restrained category.
- Properly designed and detailed FEP connections, can develop appreciable plastic rotation of 4% and up to 10%. On the other hand, FEP connections mostly fail at ultimate moment, hence, they possess no practical post-capping rotational capacity.
- FEP connections possess a median hardening stiffness of 4.5% which large compared to fully-rigid welded connections.
- The loading protocol does not seem to affect the ductility of the connection but cyclic loading may increase the magnitude of hardening.
- Stainless steel is a viable option for improving the connection ductility by at least 40%.

The assessment herein is based on response parameters deduced based on a systematic procedure that is explicitly described and can be replicated. Nonetheless, it is worth noting that other valid methodologies available in literature can be used to deduce these parameters. While, these methodologies may yield values that vary from the ones presented herein, these variations are not expected to be significant and the findings presented herein remain valid.

Finally, to support the development of modeling guidelines, acceptance criteria and system-level uncertainty quantification studies as part of the performance-based framework, a lognormal probability distribution is fitted to the distribution of each of the response parameters. Table 2 summarizes the parameters of the fitted distribution, μ_x and $\sigma_{\ln(x)}$, for different connection groups, where μ_x is the central tendency (median) of a given parameter x and $\sigma_{\ln(x)}$ is the standard deviation of the associated normal distribution.

Table 2. Summary of response parameters based on lognormal probability distribution

Connection group	Median, μ_x					
	α	β	K_s/K_e	θ_y	θ_p	θ_f
Bare steel + I-shaped + Major + Monotonic	0.32	4.81	4.1%	0.22%	4.22%	5.17%
Bare steel + I-shaped + Major + Cyclic	0.30	3.05	7.2%	0.41%	3.16%	3.69%
Bare steel + I-shaped + Minor	0.19	1.32	9.7%	0.39%	6.15%	4.86%
Bare steel + HSS	0.13	1.29	5.9%	0.29%	6.00%	1.82%
Bare steel splices	0.28	12.36	4.5%	0.11%	1.81%	1.09%
Bare stainless steel + I-shaped + Major	0.34	4.63	2.8%	0.27%	9.83%	12.15%
Composite+ I-shaped + Major	0.78	12.78	4.5%	0.22%	2.50%	3.24%
	Dispersion, $\sigma_{\ln(x)}$					
Bare steel + I-shaped + Major + Monotonic	0.47	0.91	0.68	0.86	0.55	0.58
Bare steel + I-shaped + Major + Cyclic	0.54	0.84	0.86	0.62	0.82	0.87
Bare steel + I-shaped + Minor	0.78	1.43	0.97	1.39	0.90	0.92
Bare steel + HSS	0.43	0.59	0.48	0.72	0.31	0.23
Bare steel splices	0.66	1.58	0.68	1.10	0.63	0.95
Bare stainless steel + I-shaped + Major	0.11	0.98	0.68	0.93	0.41	0.37
Composite+ I-shaped + Major	0.35	0.63	0.74	0.69	0.59	0.51

Data Availability Statement

The described experimental database as well as the deduced response parameters are publicly available in the following GitHub repository (https://github.com/amaelkady/SRConED).

References

[1] Mak, L. and A. Elkady, Experimental Database for Steel Flush End-Plate Connections. Journal of Structural Engineering, 2021. **147**(7): p. 04721006 DOI: 10.1061/(ASCE)ST.1943-541X.0003064.

[2] Nethercot, D.A., Steel beam to column connections - a review of test data and their applicability to the evaluation of the joint behaviour of the performance of steel frames, 1984.Report No. RR1084, University of Sheffield: Sheffield, UK.

[3] Kishi, N. and W.-F. Chen, Data base of steel beam-to-column connections, 1986.Report No. CE-STR-86-26, Structural Engineering Area, School of Civil Engineering, Purdue University: Indiana, USA.

[4] Chen, W.-F. and N. Kishi, Semi Rigid Steel Beam to Column Connections: Database and Modeling. Journal of Structural Engineering, 1989. **115**(1) DOI: 10.1061/(ASCE)0733-9445(1989)115:1(105).

[5] Abdalla, K.M. and W.-F. Chen, Expanded Database of Semi-Rigid Steel Connections. Computers & Structures, 1995. **56**(4): p. 553-564 DOI: 10.1016/0045-7949(94)00558-K.

[6] Weynand, K., et al. SERICON – A Databank for Tests on Semi-Rigid Joints. in COST C1: Control of the Semi-Rigid Behavior of Civil Engineering Structural Connections. 1999. Office for Official Publications of the European Communities.

[7] Lignos, D.G. and H. Krawinkler, Deterioration Modeling of Steel Components in Support of Collapse Prediction of Steel Moment Frames under Earthquake Loading. Journal of Structural Engineering, 2011. **137**(11): p. 1291-1302 DOI: 10.1061/(ASCE)ST.1943-541X.0000376.

[8] NIST/ATC, Recommended Modeling Parameters and Acceptance Criteria for Nonlinear Analysis in Support of Seismic Evaluation, Retrofit, and Design 2018.NIST GCR 17-917-

45, Prepared for the U.S. Department of Commerce and the National Institute of Standards and Technology (NIST) by the Applied Technology Council (ATC).

[9] ASCE, Seismic Evaluation and Retrofit of Existing Buildings. 2017, American Society of Civil Engineers: Reston, VA.

[10] Ostrander, J.R., An Experimental Investigation of End Plate Connections, in Department of Civil Engineering. 1970, University of Saskatchewan: Saskatchewan, Canada.

[11] Qiang, X., et al., Behaviour of Beam-to-Column High Strength Steel Endplate Connections Under Fire Conditions – Part 1: Experimental Study. Engineering Structures, 2014. **64**: p. 23-38 DOI: 10.1016/j.engstruct.2014.01.028.

[12] CEN, Eurocode 3 - Design of Steel Structures, Part 1-8: Design of Joints. 2005, European Committee for Standardization: Brussels, Belgium.

[13] AISC, Specification for Structural Steel Buildings. 2016, American Institute for Steel Construction: Chicago, IL.

[14] Brown, N.D. and D. Anderson, Structural Properties of Composite Major Axis End Plate Connections. Journal of Constructional Steel Research, 2001. **57**(3): p. 327-349 DOI: 10.1016/S0143-974X(00)00034-1.

[15] Srouji, R., Yield-line analysis of end-plate connections with bolt force predictions. 1983, University of Oklahoma: Oklahoma, USA.

[16] Pan, J., et al., Initial Rotational Atiffness of Minor-Axis Flush End-Plate Connections. Advances in Mechanical Engineering, 2018. **10**(1): p. 1687814017745397 DOI: 10.1177/1687814017745397.

[17] Bahaari, M.R. and A.N. Sherbourne, Behavior of eight-bolt large capacity end plate connections. Computers & Structures, 2000. **77**(3): p. 315-325 DOI: 10.1016/S0045-7949(99)00218-7.

[18] Aggarwal, A.K., Comparative Tests on End Plate Beam-to-Column Connections. Journal of Constructional Steel Research, 1994. **30**(2): p. 151-175 DOI: 10.1016/0143-974X(94)90048-5.

[19] El-Jisr, H., et al., Composite Steel Beam Database for Seismic Design and Performance Assessment of Composite-Steel Moment-Resisting Frame Systems. Bulletin of Earthquake Engineering, 2019. **17**(1): p. 3015-3039 DOI: 10.1007/s10518-019-00564-w.

[20] Elkady, A. and D.G. Lignos, Modeling of the Composite Action in Fully Restrained Beam-to-Column Connections: Implications in the Seismic Design and Collapse Capacity of Steel Special Moment Frames. Earthquake Engineering & Structural Dynamics, 2014. **43**(13): p. 1935-1954 DOI: 10.1002/eqe.2430.

[21] Flores, F.X., et al., Influence of the Gravity Framing System on the Collapse Performance of Special Steel Moment Frames. Journal of Constructional Steel Research, 2014. **101**(0): p. 351-362 DOI: 10.1016/j.jcsr.2014.05.020.

[22] Elkady, A. and D.G. Lignos, Effect of Gravity Framing on the Overstrength and Collapse Capacity of Steel Frame Buildings with Perimeter Special Moment Frames. Earthquake Engineering & Structural Dynamics, 2015. **44**(8): p. 1289–1307 DOI: 10.1002/eqe.2519.

[23] Davison, J.B., et al., Rotational Stiffness Characteristics of Steel Beam-to-Column Connections. Journal of Constructional Steel Research, 1987. **8**(1): p. 17-54 DOI: 10.1016/0143-974X(87)90052-6.

[24] Krawinkler, H., Shear in Beam-Column Joints in Seismic Design of Steel Frames. Engineering Journal, 1978. **15**(3): p. 82-91.

[25] PEER/ATC, Modeling and Acceptance Criteria for Seismic Design and Analysis of Tall Buildings. 2010, Prepared for Pacific Earthquake Engineering Research Center (PEER) by Applied Technology Council (ATC): Redwood City, CA.

[26] Coelho, A.M.G. and F.S.K. Bijlaard, Experimental behaviour of high strength steel end-plate connections. Journal of Constructional Steel Research, 2007. **63**(9): p. 1228-1240 DOI: 10.1016/j.jcsr.2006.11.010.

[27] Elflah, M., et al., Behaviour of stainless steel beam-to-column joints — Part 1: Experimental investigation. Journal of Constructional Steel Research, 2019. **152**: p. 183-193 DOI: 10.1016/j.jcsr.2018.02.040.

[28] Landolfo, R., et al. EQUALJOINTS PLUS-Volume with pre-normative design recommendations for seismically qualified steel joints. 2018. ECCS.

[29] Kishi, N., et al. Four-parameter power model for M-θr curves of end-plate connections. in Connections in steel structures V: Innovative steel connections. 2004. Amsterdam, Netherlands: ECCS/AISC.

[30] Richard, R.M. and B.J. Abbott, Versatile Elastic-Plastic Stress-Strain Formula. Journal of the Engineering Mechanics Division, 1975. **101**(4): p. 511-515 DOI: 10.1061/JMCEA3.0002047.

[31] Menegotto, M. and P.E. Pinto. Method of Analysis for Cyclically Loaded RC Frames Including Changes in Geometry and Non-elastic Behaviour of Elements Under Combined Normal Force and Bending. in IABSE Congress Reports of the Working Commission. 1973.

[32] Landolfo, R., European seismic prequalification of steel beam-to-column joints: EQUALJOINTS and EQUALJOINTS-Plus projects. Journal of Constructional Steel Research, 2022. **192**: p. 107238 DOI: 10.1016/j.jcsr.2022.107238.

[33] Lignos, D.G., et al., Proposed Updates to the ASCE 41 Nonlinear Modeling Parameters for Wide-Flange Steel Columns in Support of Performance-based Seismic Engineering. Journal of Structural Engineering, 2019. **145**(9): p. 04019083 DOI: 10.1061/(ASCE)ST.1943-541X.0002353.

[34] Suzuki, Y. and D.G. Lignos. Large Scale Collapse Experiments of Wide-Flange Steel Beam-Columns. in 8th International Conference on Behavior of Steel Structures in Seismic Areas. 2015. Shanghai, China.

[35] Elkady, A. and D.G. Lignos. Full-Scale Cyclic Testing of Deep Slender Wide-Flange Steel Beam-Columns under Unidirectional and Bidirectional Lateral Drift Demands. in 16th World Conference on Earthquake Engineering. 2017. Santiago, Chile.

[36] Ostrowski, K. and A. Kozłowski, Rotation Capacity of Bolted Flush End-Plate Stiffened Beam-to-Column Connection. Civil and Environmental Engineering Reports, 2017. **25**(2): p. 173-184 DOI: 10.1515/ceer-2017-0028.

[37] Bregoli, G., et al., Static and dynamic tests on steel joints equipped with novel structural details for progressive collapse mitigation. Engineering Structures, 2021. **232**: p. 111829 DOI: 10.1016/j.engstruct.2020.111829.

[38] Wang, J., et al., Progressive collapse analysis of stainless steel composite frames with beam-to-column endplate connections. Steel and Composite Structures, 2020. **36**(4): p. 427-446 DOI: 10.12989/SCS.2020.36.4.427.